Modeling the ternary chalcogenide Na_2MoSe_4 from first-principles*

Etienne Palos,[1,2,†] Armando Reyes-Serrato,[2,3] Gabriel Alonso-Nuñez,[2] and J. Guerrero Sánchez[2,‡]

[1] *Department of Chemistry and Biochemistry, University of California San Diego, La Jolla, CA 92093, USA*
[2] *Centro de Nanociencias y Nanotecnología, Universidad Nacional Autónoma de México, Ensenada B.C., 22800, México*
[3] *Donostia International Physics Center, P. Manuel de Lardizabal 4, 20018 Donostia-San Sebastián, Spain.*

(Dated: July 1, 2020)

In the ongoing pursuit of inorganic compounds suitable for solid-state devices, transition metal chalcogenides have received heightened attention due to their physical and chemical properties. Recently, alkali-ion transition metal chalcogenides have been explored as promising candidates to be applied in optoelectronics, photovoltaics and energy storage devices. In this work, we present a comprehensive theoretical study of sodium molybdenum selenide (Na_2MoSe_4). First-principles computations were performed on a set of hypothetical crystal structures to determine the ground state and electronic properties of Na_2MoSe_4. We find that the equilibrium structure of Na_2MoSe_4 is a simple orthorhombic (oP) lattice, with space group $Pnma$, as evidenced by thermodynamics. Electronic structure computations reveal that three phases are semiconducting, while one (cF) is metallic. Relativistic effects and Coulomb interaction of localized electrons were assessed for the oP phase, and found to have a negligible influence on the band strucutre. Finally, meta-GGA computations were performed to model the band structure of primitive orthorhombic Na_2MoSe_4 at a predictive level. We employ the Tran-Blaha modified Becke-Johnson potential to demonstrate that oP Na_2MoSe_4 is a semiconductor with a direct bandgap of 0.53 eV at the Γ point. Our results provide a foundation for future studies concerned with the modeling of inorganic and hybrid organic-inorganic materials chemically analogous to Na_2MoSe_4.

I. INTRODUCTION

In recent years, a class of ternary chalcogenides known as alkali-metal(ion) transition-metal (and post transition metal) chalcogenides have presented a new landscape of opportunities in solid-state physics and chemistry. These materials, with general composition AMX_n where A is an alkali metal, can be obtained by facile solid-state reactions or by intercalation of a A^+ in a MX_n lattice [1]. This, and the fact that they are well known ionic conductors, make them an attractive class of inorganic compounds [2, 3]. In this scene, Kanatzadis and coworkers have shone light on the fundamental chemistry of these compounds, discovering systems as different as semi- and superconductors [4, 5]. Regarding alkali metal transition selenides, partirularly, we highlight the discovery of the layered metal $NaCu_6Se_4$ with mixed valency [6], the mixed-valent two-dimensional metal $NaCu_4Se_3$ [7] and the two-dimensional metal $NaCu_4Se_4$, which presents high hole mobility and giant magnetoresistence [8].

On another note, AMX_n semiconductors are also gaining traction. In 2018, Z. Xia *et al* [9] have discussed the chemistry of a new alakali-transition metal chalcogenide, $CsCu_5Se_3$. This caesium copper selenide, grown via the solvothermal method, is a pseudo-direct bandgap semiconductor with a bandgap of 1 eV. It crystallizes in the oP lattice, space group $Pmma$ (No. 51). Authors also explored the complete the family of materials by synthesizing and characterizing $CsCu_5S_3$ and proposing $CsCu_5Te_3$. Since then, an α phase of $CsCu_5Se_3$ has been achieved and proposed as a high-performance thermoelectric [10] and an *ab-initio* study treats the defect physics in $CsCu_5Se_3$ and its potential in optoelectronics [11]. In a recent review on chalcogenides for photovoltaic applications, $CsCu_5Se_3$ and other new chalcogenides are compared to their oxide analogs [12], to highlight opportunities for new materials.

Recent advances worth highlighting include the emergence of a new class of transition metal chalcogenide perovksites. The interplay between alkali-metal (A^+) and MX chemistry promises solar-cell absorbers with electronic properties on a par with those of Hybrid perovskites [13–15]. One of the major advantages of TMC perovskites is high resistence to decomposition [16, 17], as well as their malleable compositional, structural and electrical and optical properties.

In this work, we aim to model Na_2MoSe_4 (See Fig. S1), a molecule chemically analogous to the well known sodium molybdate (Na_2MoO_4) [18], in the solid state. The following question arises: what will be the crystal structure of Na_2MoSe_4? The answer is not obvious, as molecular Na_2MoSe_4 is as related to Na_2MoO_4 as it is to Cs_2WS_4 [19]. Additionally, upon modeling Na_2MoSe_4, we will gain insights into the physics of its crystalline relatives. To this end, we employ a crystal structure prediction method combined with Kohn-Sham Density Functional Theory (DFT) to determine the ground state properties of this alkali metal transition metal chalcogenide. Our crystal structure prediction is based on the generation of hypothetical candidates through the ionic substitution of experimentally known analogs of Na-Mo-Se compounds. We demonstrate that Na_2MoSe_4 is a direct bandgap semiconductor with simple orthorhombic

* Supplementary information available

† epalos@ucsd.edu
‡ guerrero@cnyn.unam.mx

(oP) structure, $Pnma$ space group.

II. METHODS

A. Crystal Structure Prediction

To address the issue of structure determination, we followed the crystal structure prediction method of Hautier *et al* [20] based on data mined ionic substitutions. It has been demonstrated that the method of data mined ionic substitutions can generate likely crystal structures at a fraction of the computational cost of evolutionary algorithms [21], due to the fact that the substitutions are generated posterior to the analysis of existing crystal structures listed in the Inorganic Crystal Structure Database (ICSD). For the reader's convenience, we briefly outline the data mining + ionic substitution (DM+IS) methodology in the supplementary section.

Our DM+IS search generated over sixty-five hypothetical sodium molybdenum selenide structures, of which twenty-one present our hypothesized stoichiometry. The list of Na_2MoSe_4 candidates is found in Table S1 along with other hypothetical Na-Mo-Se structures have been made public in the Materials Project Database [22] and can be downloaded directly from our repository [23]. Here, we focus our attention to the four candidates with highest likelihood of existing in their predicted space groups.

B. Density Functional Theory Computations

Our first-principles computations based on Kohn-Sham Density Functional Theory (DFT) were carried out in the Quantum ESPRESSO package [24, 25]. We employ the General Gradient Approximation (GGA) functional with corrected-for-solids Perdew-Burke-Ernzerhof (PBEsol) parametrization for the exchange-correlation interactions [26]. It has been shown that the PBEsol is better suited to approximate lattice constants and surface energies when compared to PBE and LDA [27–29]. The ground state structures were determined by varying the volume isotropically, to control symmetry while fully relaxing atomic positions under a tolerance of 13.605×10^{-5} eV/atom for total energy and net forces of 0.025 eV·Å^{-1} per atom. These computations were performed using ultrasoft pseudopotentials (USP) developed by Dal Corso [30], with a plane-wave kinetic energy cutoff of 40 Ry (544 eV), charge density cutoff f of 320 Ry (4,354 eV) and a convergence threshold of 1×10^{-8} eV for self-consistency. Longe-range Grimme D2 Van der Waals interactions were included [31]. Monkhorst-Pack Γ-centered integration grids were used to sample the first Brillouin Zone [32]. For structural optimization computations of the cF, oF, oP and mC phases, integration grids of $6 \times 6 \times 4$, $8 \times 6 \times 5$, $6 \times 8 \times 4$, $5 \times 5 \times 4$ were used, respectively. To model the electronic structure we then increased the density of the k-points integration grids to $24 \times 28 \times 20$ (cF), $32 \times 24 \times 20$ (oF), $24 \times 32 \times 18$ (oP) and $30 \times 30 \times 24$ (mC).

The General Gradient Approximation fails to predict the fundamental bandgap of semiconductors. Therefore, we then model the electronic band structure of the favored phase by performing meta-GGA (MGGA) calculations using the the semilocal Trahn-Blaha modified Becke-Johnson (TB-mBJ) exchange potential [33]. In order to obtain optimal results, our TB-mBJ computations were carried out in the framework of the Augmetnted Planewave plus Local Orbital (APW+lo) method as implemented in the all-electron code Wien2k[34].

III. RESULTS

A. Candidate structures

The structures considered in detail are: a face centered cubic (cF) phase with space group $Fd\text{-}3m$ (227), a face centered orthorhombic (oF) with space group $Fddd$ (70), a primitive orthorhombic (oP) with space group $Pnma$ (62) and a base centered monoclinic (mC) with space group $C2/m$ (12). The unit cells are sketched in Fig. 1 (a)-(d). The structural details for the evaluated systems are shown in Table I, which includes the raw (generated) DM+IS and the computed (equilibrium) parameters. From the obtained results it is clear that the equilibrium volume changes significantly with respect to the DM+IS volume, with the exception of the oP structure. For example, $\Delta V^{oP} = 2\%$ versus $\Delta V^{cF} = 26\%$. Since we have unit cells with different number of atoms, to formally asses which of the candidates is the favored ground state phase of Na_2MoSe_4, we proceed to calculate the formation enthalpy $\Delta H^s_{f(AMX)}$. Thus, Eq. (1) reads

$$\Delta H^s_{f(AMX)} = U^s_{(AMX)} - \sum_i^3 N_i \mu^s_i, \qquad (1)$$

where $U^s_{(AMX)}$ is the total energy of our ternary compound, N_i is the number of atoms of a constituent i with chemical potential μ_i in solid phase. The chemical potentials μ for the constituent species were calculated based on DFT energies of their equilibrium crystal structures under the same relaxation criteria and convergence thresholds as the Na_2MoSe_4 candidates. Additionally, analysis was cross-checked by fully relaxing all candidate structures at the PBE level. No significant changes on the lattice parameters were found. The values for $\Delta H^s_{f(AMX)}$ are shown in Table II. Note that oP is the favored phase of the selenide with ΔH^s_f values of -5.14 (PBEsol) and -5.11 (PBE) eV per formula unit (eV/f.u.). We find these relative formation enthalpies to be in good agreement, as the relative error between the PBE/PBEsol calculations is less than 2% for all phases with the exception of the least stable cF, in which a larger discrepancy is observed.

TABLE I. Predicted and optimized lattice parameters for the Na_2MoSe_4 candidate structures computed at the GGA-(PBEsol) level of theory.

System	**a** (Å)	**b** (Å)	**c** (Å)	V (Å^3)	α	β	γ
cF: *Fd-3m* (227)							
DM+IS	6.44	6.44	9.11	188.89	45	45	90
This work	8.14	8.14	11.51	238.76	45	45	90
oF: *Fddd* (70)							
DM+IS	6.31	8.39	10.85	223.77	130	149	56
This work	7.71	10.24	13.26	273.38	130	149	56
oP: *Pnma* (62)							
DM+IS	9.32	6.84	12.08	770.49	90	90	90
This work	9.12	6.69	11.81	753.92	90	90	90
mC: *C2/m* (12)							
DM+IS	6.88	6.08	7.54	254.92	90	67	63
This work	7.78	6.88	8.52	368.58	90	67	63

TABLE II. Formation enthalpies ΔH_f for Na_2MoSe_4 candidate structures calculated using the GGA(PBEsol) and GGA(PBE) computed energies. Here, ΔH_f is shown in eV per formula unit (eV/f.u.) and per atom (eV/atom).

System	ΔH_f (eV/f.u.)	ΔH_f (eV/atom)
cF		
PBEsol	-4.39	-0.63
PBE	-4.02	-0.57
oF		
PBEsol	-4.90	-0.70
PBE	-4.83	-0.69
oP		
PBEsol	-5.14	-0.73
PBE	-5.11	-0.73
mC		
PBEsol	-5.03	-0.72
PBE	-4.91	-0.70

This is reminiscent of the Cs pervoskite $CsPbBr_3$, where through cooling, it undergoes a transition from a cubic to an orthorhombic lattice [35]. We encourage further studies to calculate the phonon band structure for the metastable phases, as we recognize the importance of these calculations to assess its dynamical stability. Here, our scope is to determine the most energetically stable structure for the already synthesized Na_2MoSe_4 compound [36, 37], and calculate its electronic properties. Once the most stable phase is determined, we focus our attention only to the *oP* phase with *Pnma* space group. To further cross check the ground state of the *Pnma* candidate, we take the initial (DM+IS) structure and optimize it at the APW+lo/PBEsol level of theory.

The calculated lattice parameter is $a = 9.21$ Å, which is in agreement with our pw(pseudo-potential) computed lattice constant $a = 9.12$, with an absolute error $e_a =\leq 1\%$. At V_0, the bulk modulus for Na_2MoSe_4 is $B_0 = 56.07$ GPa with a numerical derivative of $B_0' = 4.41$.

Due to the fact that the hypothetical crystal structures were generated from chemical analogs, it is reasonable to infer that the true equilibrium structure of our material (*oP*) should result isostructural to other materials governed by same chemical principles (e.g. valency, electronegativity, position within the periodic table etc.). Furthermore, it is inferred that compounds governed by the same chemical principles as Na_2MoSe_4 will also be favored in the *oP* lattice. This is in fact the reasoning and strength behind probabilistic models for crystal structure prediction. [38]. Therefore, the probability P of a material to exist in a specific crystal system (e.g. *oP* (*Pnma*)) will be influenced by the size of the known isostructural family[20, 38–40]. We match our evaluated structures to their analogs. First, we found our least stable candidate $cF(Fd-3m)$ to be isostructural to the stable phase of Na_2MoO_4 [ICSD No. 44523]. The metastable phase of Na_2MoO_4 [ICSD No. 151971] is characterized by the *Fddd* space group and isostructural to our *oF* candidate. The *mC* candidate is isostructural to the molecular crystal K_2MoO_4 [ICSD No. 16154]. Lastly, our most stable *oP* phase is isostructural to (or based on) K_2MoS_4 [ICSD No. 409563]. Notably, the following alkali-ion transition metal chalcogenides have been synthesized and are isostructural to Na_2MoSe_4 with *oP*(*Pnma*) symmetry: K_2MoS_4, Cs_2MoSe_4, Rb_2MoSe_4, Cs_2MoS_4, Rb_2MoS_4, K_2WSe_4 and Rb_2WS_4 [41–45] and could potentially be intrinsic semiconductors. Additionally, hybrid organic/inorganic members of the family R_2MX_4 (e.g. R = CH_3NH_3 ; M = Mo,W ; X = S, Se) have also been reported to be stable in the *oP* phase [46, 47]. Note, throughout the A_2/R_2MX_4 family, X is either S or Se. To the best of our knowledge, no theoretical studies of these materials are available in the literature. Given the electronic structure of Na_2MoSe_4 and τ_4 (see section VI), it results of interest to the broader community to understand the physics and chemistry of the *oP* A/R_2MX_4 compounds and their potential applications. Hence, we intend for our work to serve as a primer for future theoretical and experimental studies on the structural and electronic properties of both the inorganic and hybrid organic-inorganic analogs of Na_2MoSe_4. With respect to the question posed in the introduction; in the solid-state, the stable phase of Na_2MoSe_4 is isostructural to Cs_2WS_4 (*oP*) and not Na_2MoO_4 (*cF*).

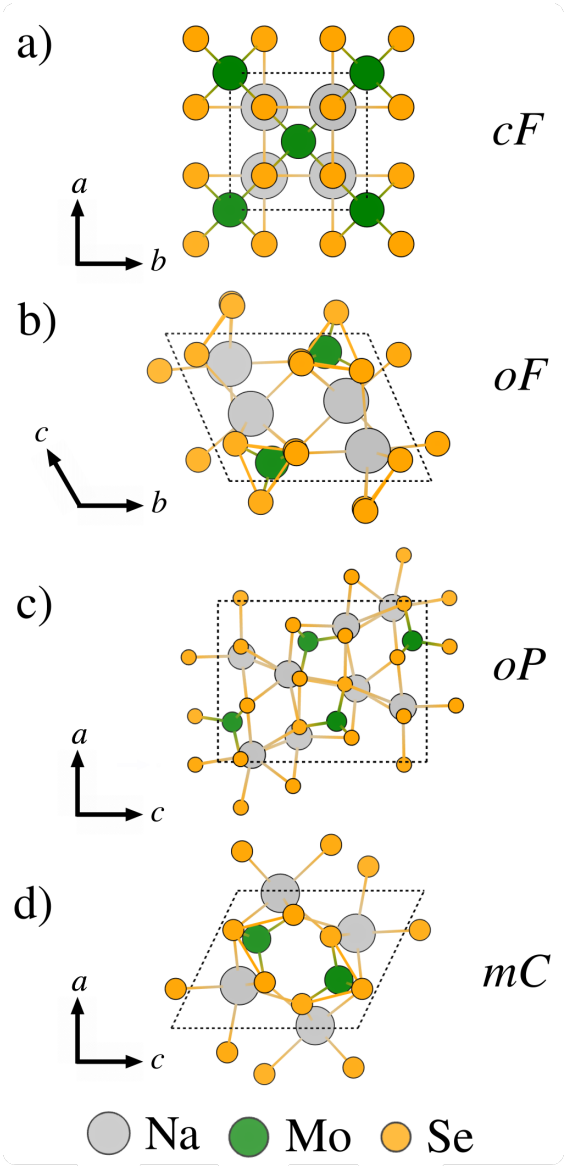

FIG. 1. Sketch of the candidate structure unit cells for Na_2MoSe_4. The candidates are labeled by their lattice type (a) face centered cubic cF, (b) face centered orthorhombic oF, (c) simple orthorhombic oP and (d) base centered monoclinic mC. Na, Mo and Se are depicted as grey, green and orange circles, respectively.

B. Structure and symmetry of orthorhombic sodium molybdenum selenide

The disodium molybdenum tetraselenide, which can be written as $Na_2[MoSe_4]$, is a molecular crystal favored to grow in the simple orthorhombic (oP) crystal system with space group $Pnma$ (No. 62), as shown in Fig. 2. It has inversion symmetry, with eight symmetry operations. In Figure 2-a, an illustration of the frontal and isometric views are shown. The Na_2MoSe_4 structure is three-dimensional, (i.e. there are no van der Waals gaps)

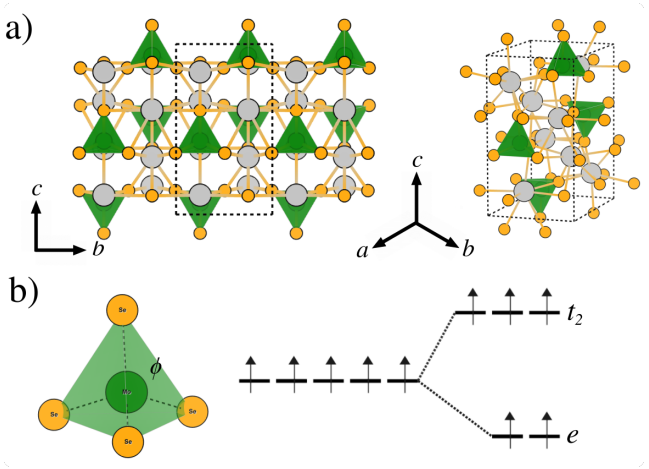

FIG. 2. Illustration of (a) isometric and front views of oP ($Pnma$) phase of Na_2MoSe_4 and (b) the $[MoSe_4]^-$ tetrahedron with a schematic illustration of the tetrahedral crystal field that splits the Mo $4d_5$ orbitals into two groups, namely t_2 and e. As seen in (a) Na^+ ions are intercalated through the $MoSe_4$ tetrahedral layers.

with two equivalent Na^{1+} sites. Note that Mo^{6+} is in tetrahedral coordination τ_4 (i.e. $\tau_4 = 1$), bonded to four Se^{2-}atoms at each vertex. There is no Mo-Na bond, and the Na cations are intercalated throughout the lattice. This promotes the one-dimensional (directional) growth of the $[MoSe_4]^-$ tetrahedrons. Hence, $MoSe_4$-terminated slabs can be achieved for Na conduction. Additionally, the electronic charge of Na induces a distortion in the tetrahedron (distortion index $t_4^{'} = 0.006$) yielding a slightly elongated Mo-Se bond ($d = 2.33$ Å) versus the other three ($d = 2.30$ Å), and a broadening of Se-Mo-Se bond angle ϕ from $\phi = 109.55°$ to $\phi = 115°$ as shown in Figure 2-b. The average Mo-Se bond length is $\bar{l} = 2.31$ Å. This distortion is caused by electronic charge effects of a Na^{1+} atom in proximity to one Se vertex ($r = 2.98$ Å). The distortion can be also measured by the tetrahedron edges, conformed by Se-Se inter-atomic distances. The tetrahedron edge lengths are $l = 3.778$, 3.576 and 3.793 Årespectively. The omitted length values are redundant in nature. A spread of Na-Se bond distances can be found in the two Na sites, with values ranging between 2.98 – 3.48 Å. In one Na^{1+} site, Na^{1+} is bonded in a 8-coordinate geometry to eight Se^{2-} atoms. In the other, our sodium cation is bonded in a 9-coordinate geometry to 9 Se anions. There are three nonequivalent Se^{2-} sites. In the first Se site, Se^{2-} is bonded in a single coordinate geometry to four Na^{1+} and one Mo^{6+} atom. In the second site, Se^{2-} is bonded in a 6-coordinate geometry to five Na^{1+} and one Mo^{6+} atom. In the third Se site, Se^{2-} is bonded in a 5-coordinate geometry to four Na^{1+} and one Mo^{6+} atom. Our structural analysis is in agreement with the available information for its reported analogs [41–45]. Note, the intercalation of Na atoms could favor an energetically low-cost substitution (or displacement) of cations, enabling the tunability of

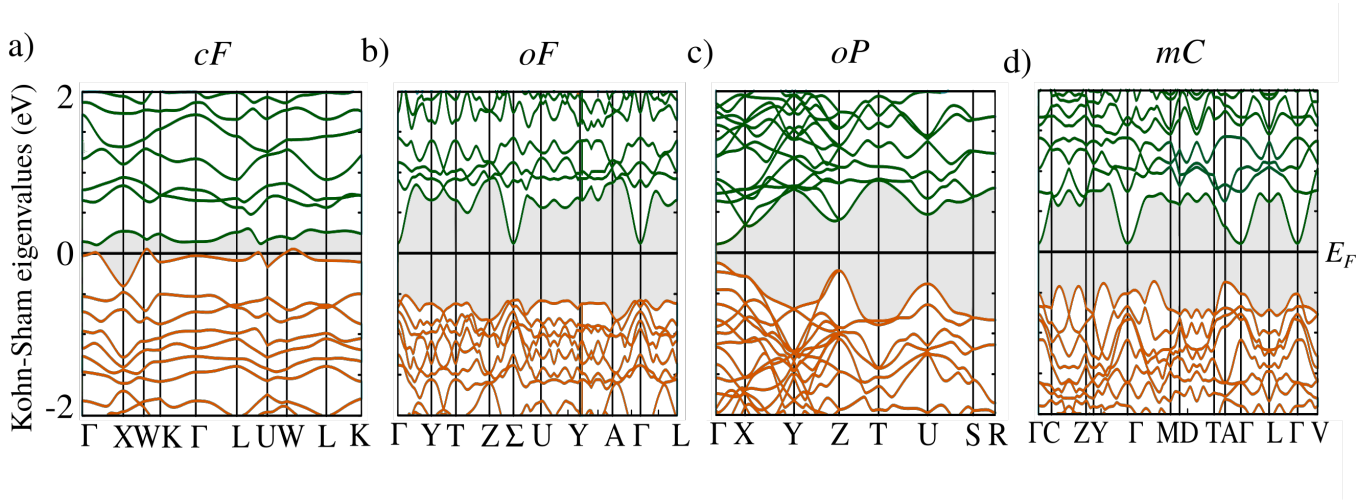

FIG. 3. The electronic band structure is shown for the (a) cF, (b) oF, (c) oP and (d) mC candidate phases of Na_2MoSe_4. The Fermi energy E_F is set to 0.

TABLE III. Band structure summary with E_g values at the GGA level of theory. To classify the phases, metals are identified by M, while D and I are employed to label direct and indirect semidoncutors. The labels k_c and k_v correspond to the points at the CBM and CVM respectively.

System	E_g^{GGA} (eV)	E_g Type	$k_c - k_v$
cF	0.00	M	$---$
oF	0.62	D	$\Gamma - \Gamma$
oP	0.24	D	$\Gamma - \Gamma$
mC	0.45	I	$A - \Gamma$

these materials' properties. Lastly, due to the structure of $Na^+[MoSe_4]^-$, it can be safely inferred that the crystal is a typical ionic conductor [45].

C. Electronic structure

The electronic structure of all candidates was investigated. Fig. 3 depicts the electronic band structure of the candidate phases of Na_2MoSe_4. Conventional k paths were used [48, 49]. In all plots, the Fermi energy (E_F) is set to zero. From the band structure plots, it is clear that one of four phases is semi-metallic; cF (Figure 3(a)), where the valence band slightly crosses the Fermi level. The remaining three are intrinsic semiconductors. The oF phase is a direct bandgap semiconductor (Figure 3 (b)), with a bandgap $E_g = 0.62$ eV at Γ, while the mC phase is an indirect bandgap ($A-\Gamma$) semiconductor with $E_g = 0.45$ eV (Figure 3(d)). Lastly, our GGA calculations show that oP Na_2MoSe_4, the stable phase, has a fundamental bandgap of $E_g^{GGA} = 0.24$ eV at Γ (Figure 3 (c)). A summary of the electronic properties computed at the GGA level is displayed in table III

Since the oP structure is energetically favored, we focus only on this phase from here in and shall refer to this phase simply as "Na_2MoSe_4".

In order to better understand the electronic band structure of Na_2MoSe_4, we adopt an alternative k path from the work of Xia *et al*[9] on oP $CsCu_5Se_3$. Note that its band dispersion is highly isotropic with clear parabolic topology at the VBM and CBM around the Γ point. Moreover, as an ionic conductor [2], it can be considered as a mixed conductor.

At this point, we analyze the nature of the Na_2MoSe_4 band structure. Let us recall that the Mo $[d^5]$ is in coordination τ_4 with Se $[4s^24p^4]$ atoms at each vertex. Given the electronic nature of our species, it is inferred that the valence bands that contribute to the E_F are composed of Se p orbitals, with mild hybridization with the Mo d orbitals. The s, p hybridization of the Mo-Se bond is common in high-spin τ_4 compounds (see Fig. Therefore, it can be said that the electronic (semiconducting) properties of the material arise mainly from the $[MoSe_4]$ sub-unit and that the effects of Na s, p electrons are negligible. However, although Na doesn't influence the band structure of the selenide, it is reasonable to believe that the displacement of Na throughout the lattice or its substitution by another ion (or molecule) could have an effect on the value of E_g. We further investigate the τ_4 subunit by treating the Se atoms as point charges around the Mo central ion, to study their bonding strength in terms of Coulombic interactions. In this sense, Crystal Field Theory (CFT) qualitatively predicts how the electrons in the Mo $4d$ orbitals respond to the effective electrostatic potential imposed by its neighboring Se atoms. In τ_4, the initial five-fold degeneracy of the $4d$ orbitals will break. This will give rise to the the orbital groups t_2 orbitals (d_{xy}, d_{yz}, d_{yz}) and the e orbitals ($d_{x^2-y^2}, d_{z^2}$). A schematic illustration of an idealized τ_4 CF is shown in the right hand side of Figure 2(b). The qualitative CFT analysis indicates that spin orbit coupling (SOC) effects in Na_2MoSe_4 are weak [50].

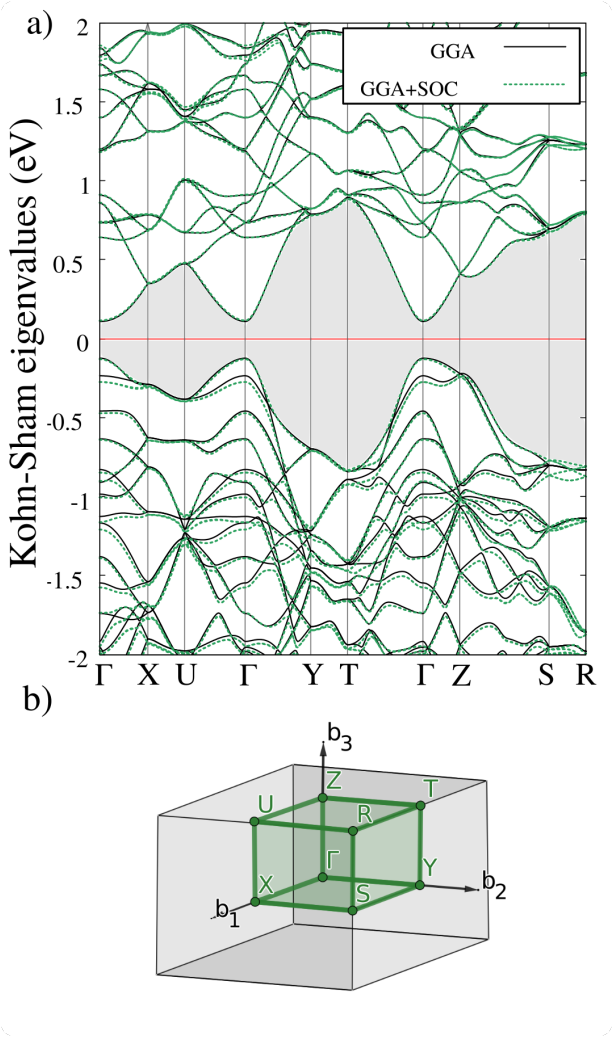

FIG. 4. Electronic band structure of oP Na_2MoSe_4 is shown in (a) modeled at the GGA (black - solid) and GGA+SOC (green - dashed) levels. The irreducible Brillouin zone and k-path for the oP lattice is shown in (b).

We then perform full-relativistic calculations to model the band structure and the effects of the spin-orbit coupling term. To see effects of SOC effect on the band structure, we adopt an alternative path of integration along the FBZ. The band structure of Na_2MoSe_4 with and without SOC $\Gamma \rightarrow X \rightarrow U \rightarrow \Gamma \rightarrow Y \rightarrow T \rightarrow \Gamma \rightarrow Z \rightarrow S \rightarrow R$ k-path (Figure 4). The FBZ is shown in Figure 4 (b). As expected, no change was observed in E_g upon calculating the band structure confirming the weak (essentially null) SOC effect. As we have seen, Na_2MoSe_4 has relatives where the A^+ cation is either Rb or Cs. Therefore, although SOC is weak in the Na member of the family, it is necessary to account for relativistic effects when modeling the band structure [35].

For completeness, we also plot the band structure by introducing an empirical Hubbard potential (GGA+U ; $U = U_{eff} = 3.5$ eV [51]) to test for Coulomb effects in Mo d electrons (see Supplementary Information, Fig. S3.). No significant change was found as well, so there is not an apparent strong electronic correlation in the Na_2MoSe_4 structure.

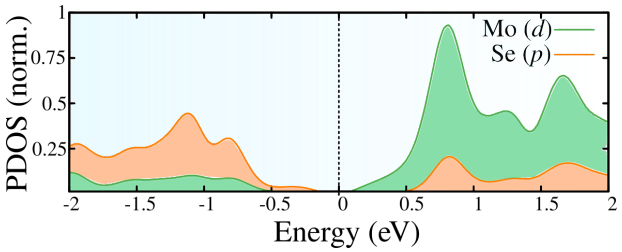

FIG. 5. Projected density of states is shown for the valence orbitals Mo and Se. Here, E_F is at 0, indicated by a dashed line.

In the region, $U \rightarrow \Gamma \rightarrow Y$, the electron and hole effective masses m_h^* and m_e^* are expected to be constant, as the dispersion of $E(k)$ near Γ is linear .

In Fig. 5, the projected DOS (PDOS) is shown for the Mo d, Se p and Na s electrons. Clearly the Na s states do not contribute near the Fermi level. The hybridized d/p orbitals; Mo d states (note $0 \leq E_F \leq 2$ eV) and the Se p states are the ones dominating the contributions around the Fermi level. In other words, in the vicinity of E_F, the orbital composition of the conduction bands are Mo d while the valence bands are Se p. Note that higher PDOS is observed above the Fermi level, due to the unoccupied states in the shells. A decomposition of the summed Mo d orbitals can be found in the supplemental material.

Although ground state GGA computations can provide a reasonable first approximation to model the electronic structure of a material, they systemically fail to predict the fundamental value of E_g. Hence, a precise approach such as the use of meta-GGA, hybrid functionals or the many-body perturbation theory method GW is desired. To achieve a predictive level, we have opted for the Meta-GGA, Trahn-Blaha modified Becke-Johnson potential (TB-mBJ), designed and proven to yield robust results comparable to those obtained by other theoretical treatments and observed in experiments[33, 52–57]. In the present scenario, the use of TB-mBJ is considered adequate as no further corrections for correlation or spin-orbit coupling are are needed (since the band topology and E_g do not change). Details regarding the TB-mBJ exchange potential are provided in the Supplementary Information file [33].

The band structure of oP Na_2MoSe_4 calculated with the semilocal potential TB-mBJ is shown in Fig. 6. Note that the band topology is invariant and located at Γ (Figure 4), but a widening of the bandgap is observed. When modeling the electronic band structure of Na_2MoSe_4 with the modified Becke-Johnson potential through an all-electron treatment, $E_g^{TB-mBJ} = 0.53$ eV at Γ. The CBs are composed mainly of Mo d states whereas the Se p states, depicted as larger points, dominate the VB contributions, in agreement with the pDOS in Figure 5. It is important to point out that TB-mBJ semilocal po-

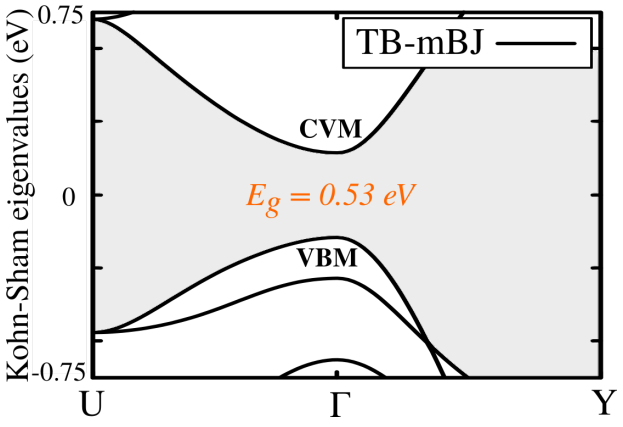

FIG. 6. Electronic band structure schematic of Na_2MoSe_4 obtained by TB-mBJ, with emphasis along $U \rightarrow \Gamma \rightarrow Y$ to better visualize the bandgap. E_F is set to zero. For the full band structure, see Fig. S4.

tential enables the modeling the electronic structures of large and chemically complex semiconducting materials as well as insulators with predictive accuracy [58, 59], and is currently considered the most accurate semilocal potential for semiconductor modeling [60, 61].

Although the bandgap isn't yet "ideal" for applications in traditional optoelectronic devices or photovoltaics, Na_2MoSe_4 with an intrinsic direct bandgap of 0.53 eV holds potential for applications in infrared optoelectronics and high-speed electronic heterostructures and devices. Since the bandgap is tunable via ionic displacement and/or substitution, a natural interest in studying these effects throughout the lattice rises. More importantly, it will be interesting to build upon the work presented and investigate the interplay between chemical composition, thermodynamic stability and electronic structure in the inorganic and hybrid relatives of Na_2MoSe_4.

IV. CONCLUSIONS

In this study, we have presented a theoretical investigation on the alkali-ion transition metal chalcogenide Na_2MoSe_4. First-principles computations based on periodic Density Functional Theory were systematically performed on a set of data-mined hypothetical crystal structures to determine their stability and model their electronic properties. The face centered cubic, face centered orthorhombic, simple orthorhombic and base centered monoclinic phases were studied in detail. The stability analysis reveals that the simple orthorhombic is the favored phase, with space group *Pnma*, therefore Na_2MoSe_4 is isostructural to Cs_2WS_4 and $(CH_3NH_3)_2MoS_4$. Additionally, the electronic band structure depicts semiconducting behaviour for three candidates, while the cubic phase is semi-metallic. The band structure of orthorhombic Na_2MoSe_4 is modeled at the meta-GGA level of theory with the Trahn-Blaha modified Becke-Johnson exchange potential, yielding a direct fundamental bandgap of 0.53 eV at Γ. Thus, this bandgap makes Na_2MoSe_4 suitable for applications in infrared optoelectronics and high speed electronics. Our analysis indicates that the qualitative physics of Na_2MoSe_4 may be transferable to *oP* chemical analogs, and raises questions regarding the interplay between the composition, energetics and band structure of similar compounds. We hope our work will serve as a first step towards the understanding of the alkali-ion transition metal chalcogenides family as well as the hybrid organic-inorganic transition metal chalcogenide semiconductors.

ACKNOWLEDGMENTS

E.I.P thanks Prof. Roald Hoffmann for insightful discussions on structure prediction and transition metal compounds. We thank DGAPA-UNAM projects IA100920 and IG200320 for partial financial support. Computations were performed in the DGCTIC-UNAM Supercomputing Center, project No. LANCAD-UNAM-DGTIC-390 and Laboratorio Nacional de Supercómputo del Sureste de México. E.I.P acknowledges CONACyT for a SNI-III assistantship under G.A.N. J.G.S acknowledges THUBAT KAAL IPICYT supercomputing center for computational resources. A.R.S. thanks DGAPA-UNAM project PAPIIT IN112917.

[1] Z. Guo, F. Sun, and W. Yuan, Chemical intercalations in layered transition metal chalcogenides: Syntheses, structures, and related properties, Crystal Growth & Design **17**, 2238 (2017), https://doi.org/10.1021/acs.cgd.7b00146.

[2] J. Rouxel, Alkali metal intercalation compounds of transition metal chalcogenides: Tx2, tx3 and tx4 chalcogenides, in *Intercalated Layered Materials*, edited by F. Lévy (Springer Netherlands, Dordrecht, 1979) pp. 201–250.

[3] D. W. Murphy, S. A. Sunshine, and S. M. Zahurak, Preparation methods for alkali metal intercalation compounds of oxides and chalcogenides, in *Chemical Physics of Intercalation*, edited by A. P. Legrandand S. Flandrois (Springer US, Boston, MA, 1987) pp. 173–179.

[4] C. D. Malliakas, D. Y. Chung, H. Claus, and M. G. Kanatzidis, Superconductivity in the narrow-gap semiconductor rbbi$_{11/3}$te$_6$, J. Am. Chem. Soc **138**, 14694 (2016).

[5] H. Chen, H. Claus, J.-K. Bao, C. C. Stoumpos, D. Y. Chung, W.-K. Kwok, and M. G. Kanatzidis, Superconductivity and structural conversion with na and k doping of the narrow-gap semiconductor csbi$_4$te$_6$, Chem. Mater **30**, 5293 (2018).

[6] M. Sturza, C. D. Malliakas, D. E. Burgaris, F. Han, D. Y. Chung, and M. G. Kanatzidis, Nacu6se4: A layered compound with mixed valency and metallic properties, Inorg. Chem. **53**, 12191 (2014).

[7] M. Sturza, D. E. Burgaris, C. D. Malliakas, F. Han, D. Y. Chung, and M. G. Kanatzidis, Mixed-valent nacu4se3: A two-dimensional metal, Inorg. Chem. **55**, 4884 (2016).

[8] H. Chen, J. N. B. Rodrigues, A. J. E. Rettie, T.-B. Song, D. G. Chica, X. Su, J.-K. Bao, D. Y. Chung, W.-K. Kwok, L. K. Wagner, and M. G. Kanatzidis, High hole mobility and nonsaturating giant magnetoresistance in the new 2d metal nacu4se4 synthesized by a unique pathway, J. Am. Chem. Soc. **141**, 635 (2019).

[9] Z. Xia, H. Fang, X. Zhang, M. S. Molokeev, R. Gautier, Q. Yan, S.-H. Wei, and K. R. Poeppelmeier, Cscu5se3: A copper-rich ternary chalcogenide semiconductor with nearly direct band gap for photovoltaic application, Chemistry of Materials **30**, 1121 (2018), https://doi.org/10.1021/acs.chemmater.7b05104.

[10] N. Ma, Y.-Y. Li, L. Chen, and L.-M. Wu, -cscu5se3: Discovery of a low-cost bulk selenide with high thermoelectric performance, Journal of the American Chemical Society **142**, 5293 (2020), pMID: 32118412, https://doi.org/10.1021/jacs.0c00062.

[11] A. Stoliaroff, S. Jobic, and C. Latouche, An ab initio perspective on the key defects of cscu5se3, a possible material for optoelectronic applications, The Journal of Physical Chemistry C **124**, 4363 (2020), https://doi.org/10.1021/acs.jpcc.9b10764.

[12] M. Buffiere, D. S. Dhawale, and F. El-Mellouhi, Chalcogenide materials and derivatives for photovoltaic applications, Energy Technology **7**, 1900819 (2019).

[13] K. Kuhar, A. Crovetto, M. Pandey, K. S. Thygesen, B. Seger, P. C. K. Vesborg, O. Hansen, I. Chorkendorff, and K. W. Jacobsen, Sulfide perovskites for solar energy conversion applications: computational screening and synthesis of the selected compound lays3, Energy Environ. Sci. **10**, 2579 (2017).

[14] S. Perera, H. Hui, C. Zhao, H. Xue, F. Sun, C. Deng, N. Gross, C. Milleville, X. Xu, D. F. Watson, B. Weinstein, Y.-Y. Sun, S. Zhang, and H. Zeng, Chalcogenide perovskites – an emerging class of ionic semiconductors, Nano Energy **22**, 129 (2016).

[15] S. Niu, H. Huyan, Y. Liu, M. Yeung, K. Ye, L. Blankemeier, T. Orvis, D. Sarkar, D. J. Singh, R. Kapadia, and J. Ravichandran, Bandgap control via structural and chemical tuning of transition metal perovskite chalcogenides, Advanced Materials **29**, 1604733, https://onlinelibrary.wiley.com/doi/pdf/10.1002/adma.201604733.

[16] Q. Sun, H. Chen, and W.-J. Yin, Do chalcogenide double perovskites work as solar cell absorbers: A first-principles study, Chem. Mater. **31**, 244 (2019).

[17] A. Swarnkar, W. J. Mir, R. Chakraborty, M. Jagadeeswararao, T. Sheikh, and A. Nag, Are chalcogenide perovskites an emerging class of semiconductors for optoelectronic properties and solar cell?, Chem. Mater. **31**, 565 (2019).

[18] National center for biotechnology information. pubchem database. sodium molybdate, cid=61424, https://pubchem.ncbi.nlm.nih.gov/compound/Sodium-molybdate (), accessed: 2020-19-04.

[19] National center for biotechnology information. pubchem database. dicesium;tungsten;tetrasulfide, cid=139072572, https://pubchem.ncbi.nlm.nih.gov/compound/139072572 (), accessed: 2020-19-04.

[20] G. Hautier, C. Fischer, V. Erlacher, A. Jain, and G. Ceder, Data mined ionic substitutions for the discovery of new compounds, Inorg. Chem. **50**, 656 (2011).

[21] A. Narayan, A. Bhutani, S. Rubeck, J. N. Eckstein, D. P. Shoemaker, and L. K. Wagner, Computational and experimental investigation for new transition metal selenides and sulfides: The importance of experimental verification for stability, Phys. Rev. B **94**, 045105 (2016).

[22] A. Jain, S. P. Ong, G. Hautier, W. Chen, W. D. Richards, S. Dacek, S. Cholia, D. Gunter, D. Skinner, G. Ceder, and K. a. Persson, The Materials Project: A materials genome approach to accelerating materials innovation, APL Materials **1**, 011002 (2013).

[23] Repository: Na$_2$mose$_4$ crystal structures and data., https://github.com/etiennepalos/Na2MoSe4, accessed: 2020-19-04.

[24] P. Gianozzi, S. Baroni, N. Bonini, M. Calandra, R. Car, C. Cavazzoni, D. Ceresoli, G. L. Chiarotti, M. Cococcioni, I. Dabo, A. D. Corso, S. de Gironcoli, S. Fabris, G. Fratesi, R. Gebauer, U. Gerstmann, C. Gougoussis, A. Kokalj, M. Lazzer, L. Martin-Samos, N. Marzari, F. Mauri, R. Mazzarello, S. Paolini, A. Pasquarello, L. Paulatto, C. Sbraccia, S. Scandolo, G. Sclauzero, A. P. Seitsonen, A. Smogunov, P. Umari, and R. M. Wentzcovitch, Quantum espresso: a modular and open-source software project for quantum simulations of materials, Journal of Physics: Condensed Matter **21**, 395502 (2017).

[25] P. Gianozzi, O. A. T. Brumme, O. Bunau, M. B. Nardelli, M. Calandra, R. Car, C. Cavazzoni, D. Ceresoli, M. Cococcioni, N. Colonna, I. Carnimeo, A. D. Corso, S. de Gironcoli, P. Delugas, R. D. Jr, A. Ferretti, A. Floris, G. Fratesi, G. Fugallo, R. Gebauer, U. Gerstmann, F. Giustino, T. Gorni, J. Jia, M. Kawamura, H.-Y. Ko, A. Kokalj, E. Kucukbenli, M. Lazzeri, M. Marsili, N. Marari, F. Mauri, N. Nguyen, H.-V. Nguyen, A. O. de-la Roza, L. Paulatto, S. Ponce, D. Rocca, R. Sabatini, B. Santra, M. Schlipf, A. Seitsonen, A. Amogunov, I. Timrov, T. Thonhauser, P. Umari, N. Vast, X. Wu, and S. Baroni, Advanced capabilities for materials modelling with quantum espresso, Journal of Physics: Condensed Matter **29**, 656 (2017).

[26] J. Perdew, A. Ruzsinsky, G. Csonka, O. A. Vydov, G. E. Scuseria, L. A. COnstantin, X. Zhou, and K. Burke, Restoring the density-gradient expansion for exchange in solids and surfaces, Physical Review Letters **100**, 136406 (2009).

[27] G. D. Nguimdoand D. P. Jourbert, A density functional (pbe, pbesol, hse06) study of the structural, electronic and optical properties of the ternary compounds agalx2 (x = s, se, te), European Physical Journal B **88**, 136406 (2014).

[28] M. Benam, N. Abdoshahi, and M. M. Sarmazdeh, Ab initio study of the effect of pressure on the structural and electronic properties of cubic laalo3 by density function theory using gga, lda and pbesol exchange correlation potentials, Physica B **446**, 32 (2014).

[29] M. D. L. Pierre, R. Orlando, L. Maschio, K. Doll, P. uliengo, and R. Dovesi, Performance of six function-

als (lda, pbe, pbesol, b3lyp, pbe0, and wc1lyp) in the simulation of vibrational and dielectric properties of crystalline compounds. the case of forsterite mg2sio4, Journal of Computational Chemistry **32**, 1775 (2011).
[30] A. D. Corso, Pseudopotentials periodic table: From h to pu, Computational Materials Science **95**, 337 (2014).
[31] S. Grimme, Semiempirical gga-type density functional constructed with a long-range dispersion correction, Journal of computational chemistry **27**, 1787 (2006).
[32] H. J. Monkhorstand J. D. Pack, Special points for brillouin-zone integrations, Phys. Rev. B **13**, 5188 (1976).
[33] F. Tranand P. Blaha, Accurate band gaps of semiconductors and insulators with a semilocal exchange-correlation potential, Phys. Rev. Lett. **102**, 226401 (2009).
[34] P. Blaha, K. Schwarz, F. Tran, R. Laskowski, G. K. H. Madsen, and L. D. Marks, Wien2k: An apw+lo program for calculating the properties of solids, The Journal of Chemical Physics **152**, 074101 (2020), https://doi.org/10.1063/1.5143061.
[35] M. G. Goestenand R. Hoffmann, Mirrors of bonding in metal halide perovskites, Journal of the American Chemical Society **140**, 12996 (2018), pMID: 30207152, https://doi.org/10.1021/jacs.8b08038.
[36] M. A. Reynoldsand S. N. Milam, Process for producing a copper thiometallate or a selenometallate material (2013), uS Patent 8,409,541.
[37] M. A. Reynolds, Process for producing a thiometallate or a selenometallate material (2015), uS Patent 8,940,268.
[38] C. C. Fischer, K. J. Tibbetts, D. Morgan, and G. Ceder, Predicting crystal structure by merging data mining with quantum mechanics, Nature Materials **5**, 641 (2006).
[39] G. Hautier, C. C. Fischer, A. Jain, T. Mueller, and G. Ceder, Finding nature's missing ternary oxide compounds using machine learning and density functional theory, Chemistry of Materials **22**, 3762 (2010), https://doi.org/10.1021/cm100795d.
[40] S. Atahan-Evrenkand A. Aspuru-Guzik, Prediction and calculation of crystal structures, Topics in Current Chemistry **345** (2014).
[41] C. Raymond, P. Dorhout, and S. Miller, Crystal structure of dicaesium tetramolybdate, cs_2mos_4, Zeitschrift fur Kristallographie - Crystalline Materials **210**, 775 (1995).
[42] J. Ellermeier, C. Nather, and W. Bensch, Rb_2mos_4, Acta Crystallographica Section C **55**, 1748 (1995).
[43] M. Emirdag-Eanesand J. A. Ibers, Crystal structure of dipotassium tetrathiomolybdate k_2mos_4, Zeitschrift fur Kristallographie - New Crystal Structures **216**, 484 (2001).
[44] D. Rohnert, C. Nather, and W. Bensch, K_2ws_4, Acta Crystallographica Section C **53**, 165 (1997).
[45] A. Mullerand W. Sievert, Rontgenographische untersuchungen und strukturchemie von chalkogenomolybdaten und - wolframaten, Zeitschrift fur Anorganische und Allgemeine Chemie **403**, 251 (1974).
[46] B. R. Srinivasan, C. Näther, A. R. Naik, and W. Bensch, Bis(methylammonium) tetrathiomolybdate(VI), Acta Crystallographica Section E **62**, m1635 (2006).
[47] B. R. Srinivasan, C. Näther, and W. Bensch, Bis(methylammonium) tetrasulfidotungstate(VI), Acta Crystallographica Section E **64**, m296 (2008).
[48] W. Setyawanand S. Curtarolo, High-throughput electronic band structure calculations: Challenges and tools, Computational Materials Science **49**, 299 (2010).
[49] Y. Hinuma, G. Pizzi, Y. Kumagai, F. Oba, and I. Tanaka, Band structure diagram paths based on crystallography, Computational Materials Science **128**, 140 (2017).
[50] R. G. Burns, *Mineralogical Applications of Crystal Field Theory, Second Edition* (Cambridge University Press, 2005) pp. 22–30.
[51] A. K., S. J. H. Montoya, J. M. Gregoire, and K. A. Persson, Robust and synthesizable photocatalysts for co_2 reduction: a data-driven materials discovery, Nature Communications **443**, 1 (2019).
[52] J. A. Camargo-Martínezand R. Baquero, Performance of the modified becke-johnson potential for semiconductors, Phys. Rev. B **86**, 195106 (2012).
[53] D. J. Singh, Electronic structure calculations with the tran-blaha modified becke-johnson density functional, Phys. Rev. B **82**, 205102 (2010).
[54] H. Jiang, Band gaps from the tran-blaha modified becke-johnson approach: A systematic investigation, The Journal of Chemical Physics **138**, 134115 (2013), https://doi.org/10.1063/1.4798706.
[55] W. Feng, D. Xiao, Y. Zhang, and Y. Yao, Half-heusler topological insulators: A first-principles study with the tran-blaha modified becke-johnson density functional, Physical Review B **82**, 235121 (2010).
[56] H. Dixit, R. Saniz, S. Cottenier, D. Lamoen, and B. Partoens, Electronic structure of transparent oxides with the tran–blaha modified becke–johnson potential, Journal of Physics: Condensed Matter **24**, 205503 (2012).
[57] D. Waroquiers, A. Lherbier, A. Miglio, M. Stankovski, S. Poncé, M. J. Oliveira, M. Giantomassi, G.-M. Rignanese, and X. Gonze, Band widths and gaps from the tran-blaha functional: Comparison with many-body perturbation theory, Physical Review B **87**, 075121 (2013).
[58] R. A. Jishi, O. B. Ta, and A. A. Sharif, Modeling of lead halide perovskites for photovoltaic applications, The Journal of Physical Chemistry C **118**, 28344 (2014).
[59] B. Traoré, G. Bouder, W. Lafargue-Dit-Hauret, X. Rocquefelte, C. Katan, F. Tran, and M. Kepenekian, Efficient and accurate calculation of band gaps of halide perovskites with the tran-blaha modified becke-johnson potential, Physical Review B **99**, 035139 (2019).
[60] F. Tranand P. Blaha, Importance of the kinetic energy density for band gap calculations in solids with density functional theory, The Journal of Physical Chemistry A **121**, 3318 (2017), pMID: 28402113, https://doi.org/10.1021/acs.jpca.7b02882.
[61] F. Tran, J. Doumont, L. Kalantari, A. Huran, M. L. Marques, and P. Blaha, Semilocal exchange-correlation potentials for solid-state calculations: Current status and future directions, Journal of Applied Physics **126**, 110902 (2019), https://doi.org/10.1063/1.5118863.